

Article

Enhanced Fracture Toughness and High-Temperature Strength of Directionally Solidified Mo-XC Alloys

Julia Becker ^{1,*}, Danio Breuer ², Iurii Bogomol ³  and Manja Krüger ¹ 

¹ Institute of Materials and Joining Technology, Otto-von-Guericke University Magdeburg, Universitätsplatz 2, 39106 Magdeburg, Germany

² Joyson Safety Systems Ignition GmbH, 39218 Schönebeck, Germany

³ High Temperature Materials and Powder Metallurgy Department, Igor Sikorsky Kyiv Polytechnic Institute, National Technical University of Ukraine "KPI", Peremogy Av. 37, 03056 Kiev, Ukraine

* Correspondence: julia.becker@ovgu.de; Tel.: +49-391-67-54572

Abstract: The present article focuses on refractory metals strengthened by ceramic phases to improve the mechanical properties at ambient temperatures as well as at high temperatures. In this work, near-eutectic, directionally solidified (DS) Mo-34TiC and Mo-27ZrC alloys are investigated with regard to their microstructures, fracture toughness at room temperature and compressive strength at high temperatures. Superior fracture toughness as well as competitive strength compared with other Mo-XC composites are achieved. Compressive tests up to 1000 °C on longitudinal and transversal specimens show the significant impact of the anisotropy on the strength.

Keywords: directional solidification; zone melting; Mo-TiC; Mo-ZrC; eutectic colonies; lamellar microstructure



Citation: Becker, J.; Breuer, D.; Bogomol, I.; Krüger, M. Enhanced Fracture Toughness and High-Temperature Strength of Directionally Solidified Mo-XC Alloys. *Crystals* **2022**, *12*, 1534. <https://doi.org/10.3390/cryst12111534>

Academic Editors: Li-Wei Tseng, Yu-Chih Tzeng and Yeong-Lin Lai

Received: 30 September 2022

Accepted: 25 October 2022

Published: 28 October 2022

Publisher's Note: MDPI stays neutral with regard to jurisdictional claims in published maps and institutional affiliations.



Copyright: © 2022 by the authors. Licensee MDPI, Basel, Switzerland. This article is an open access article distributed under the terms and conditions of the Creative Commons Attribution (CC BY) license (<https://creativecommons.org/licenses/by/4.0/>).

1. Introduction

In the last decades, the possible applications for refractory metals, such as tungsten, tantalum, niobium, titanium and molybdenum, have multiplied. Their specific properties, which include good creep resistance and strength at high temperatures, make them precious materials in energy, aerospace and medical technology [1]. Due to their high melting points and high thermal as well as electrical conductivity, ceramic phases are also becoming increasingly important for high-temperature applications. However, their advantage of low density is countered by the disadvantage of very low fracture toughness [2]. Research therefore increasingly focuses on alloys of refractory metals and ceramics, so-called cermets, combining the positive properties of both materials; thus, taking the technical development of high-temperature machines and devices to a new level.

Recent investigations focus on Mo-TiC and Mo-ZrC composites for high-temperature structural materials. In this respect, various approaches for material optimization were applied with regard to different alloy compositions and production processes. Several authors confirmed the ceramic phases as useful to increase the strength of Mo alloys.

In the early 1980s, Kohyama et al. [3] mentioned the potential of the Mo-TiC eutectic alloy for the use in walls of fusion reactors. Initial studies on the mechanical properties of Mo-TiC alloys were carried out by Kurishita et al. [4], pointing out the extremely high strength of the lamellar eutectic composite. Another series of Mo-TiC alloys with TiC additions not larger than 2 mass.% was studied by Hiraoka et al. [5], showing the effects of TiC addition on the strength and ductility at low temperature after grain growth treatment. It was shown that both yield and maximum strengths increased by TiC addition and consequently, ductility was improved. Observations on the microstructures of HIP Mo-TiC alloys with additions from 12.5 vol.% up to 75 vol.% TiC were carried out by Le Fem et al. [6], indicating an oxygen pollution leading to a composition shift regarding phase diagram predictions. Further investigations by Cédât et al. [2,7] show the microstructure of

a HIP Mo-25TiC (at.%) alloy highlighting the formation of a TiC–15at.%Mo phase at the TiC/Mo interface, in agreement with the phase diagram. Further articles show that Mo-ZrC alloys provide a similar potential as Mo-TiC alloys. In this regard, Suzuki investigated Mo-ZrC alloys processed via arc melting [8], pointing out that the microstructure consists of primary ZrC particles and a fine Mo/ZrC eutectic structure; i.e., hyper-eutectic structure. Compressive creep tests up to 1873 K indicate the dislocation creep of the Mo solid solution phase controlled by the lattice diffusion of either Mo or Zr [9]. Subsequent investigations of Suzuki et al. [9] focused on the microstructures and fracture toughness of directional solidified Mo-ZrC alloys (Mo-14Zr-11.7C and Mo-16ZrC), with fracture toughness up to 20 MPa m^{1/2}, depending on the manufacturing process.

Landwehr et al. investigated ZrC-XMo (X = 20–40 vol.%) alloys [10–12] processed via HIP, pointing out decreasing hardness, but increasing flexure strength and fracture toughness with increasing Mo phase fractions [12]. Another promising approach in terms of ceramic phases in Mo alloys is the particle hardening. There are studies by Ohser-Wiedemann et al. [13] working on TiC particle-reinforced Mo composites sintered by SPS. Powders with TiC contents between 6 and 25 vol.% were prepared by high-energy ball milling. It turns out that the addition of hard TiC particles to molybdenum leads to a significant hardness increase. As expected, the hardness increases with an increasing TiC fraction [13]. Similar ideas also exist with regard to reinforcement with ZrC investigated by Takida et al. [14–16]. The authors reported superior room and high-temperature strengths as well as much higher strength at room temperature by adding 0.8 vol.% ZrC to Mo (processed by spark plasma sintering).

Based on the investigations mentioned above, alloying with TiC is a very promising approach in order to improve the mechanical properties of ternary Mo-Si-B alloys and the density at the same time. Yoshimi et al. [17,18] developed novel TiC-added Mo-Si-B alloys with improved mechanical properties, especially fracture toughness.

Superior mechanical properties can be achieved by materials having lamellar microstructures. Preliminary studies by Hasemann et al. [19] and Bolbut et al. [20] have shown that zone melting process is a cost-effective and time-efficient manufacturing process in order to design directionally solidified molybdenum-based composites.

The approach followed in this paper is based on the pseudo-binary phase diagrams Mo/TiC and Mo/ZrC, mentioned in [2] and [10], respectively. Both systems represent a eutectic reaction with Mo at 34 at.% TiC and 27 at.% ZrC, respectively. The present article deals with the microstructure and mechanical properties of these near-eutectic Mo-XC (X = TiC, ZrC) alloys processed by directional solidification (DS) via a crucible-free zone melting technique (ZM). The characterization of the alloys was carried out using analytical methods, such as X-ray diffraction, scanning electron microscopy as well as compression and bending tests.

2. Materials and Methods

The alloy compositions chosen from the pseudo-binary phase diagrams, given in [2,11], are Mo-34TiC and Mo-27ZrC (at.%), which were processed by directional solidification via a crucible-free zone melting technique. Starting from powder mixtures of Mo, TiC/ZrC of 99.95% purity, respectively, the powders were cold pressed. The green compacts were dried under vacuum at 100–200 °C for 9 h before melting to ensure curing of the plastificator. Afterwards, the powder was compacted in an induction heated zone melting device “Crystal 206” (KPI-Kiev, Ukraine). Zone melting was performed in a high purity He atmosphere using solidification rates of 60 mm/h. The resulting DS rods are around 80 mm in length, having a diameter of about 7 mm.

For microstructure investigations, the samples were wet-grinded from 500 down to 1200 grit and the specimen surface was finished by polishing with 3 µm and 1 µm diamond suspension. The microstructural analysis was applied by means of scanning electron microscopy (SEM-FEI ESEM XL30 FEG equipped with EDS), while images were typically obtained in the BSE mode and X-ray diffraction measurements using a Bruker D8

Discover diffractometer with Bragg-Brentano geometry and an Eiger2 500K 2D detector and Cu-K $\alpha_{1,2}$ radiation (Bruker AXS GmbH, Karlsruhe, Germany). Quantitative phase analysis was performed using the Rietveld method with the Topas V6 program package (Bruker AXS GmbH, Karlsruhe/Coelho Software, Brisbane, Australia), as described in [21]. The room-temperature fracture strength was applied performing three-point bending tests on a notched bending specimen with dimensions of 2 mm \times 2 mm \times 18 mm (DIN EN ISO 23146). In the first step, the ground and polished bending specimens were provided with a pre-notch using a diamond saw, ending up with a notch geometry of 0.8 mm in depth and less than 0.2 mm in width. A “sharp crack” with a typical depth of 200 μ m and a tip radius of around 10 μ m was produced using a self-built cutting device equipped with a razor blade working with 1 μ m diamond paste. In order to control the notch depth and tip-radius, the samples were examined at defined intervals (15–20 min) using an optical microscope. Fracture toughness measurements were then performed applying a minimum number of five samples having similar notch base radii of around 10 μ m. Three-point flexure was realized using a microtest cell (Materials Testing Nano Tomography Version 3.2, Deben) at ambient temperature, with a load rate of 0.5 mm/min after preloading with 2 N. The determination of fracture toughness was carried out as described elsewhere [21]. The thermomechanical behavior was determined by constant displacement tests at a nominal strain rate of $1 \cdot 10^{-4} \text{ s}^{-1}$ in uniaxial compression at 400 $^{\circ}\text{C}$, 600 $^{\circ}\text{C}$, 800 $^{\circ}\text{C}$ and 1000 $^{\circ}\text{C}$ for Mo-34TiC; as well as 200 $^{\circ}\text{C}$, 400 $^{\circ}\text{C}$, 600 $^{\circ}\text{C}$ and 800 $^{\circ}\text{C}$ for Mo-ZrC. Due to anisotropic microstructure resulting from directional solidification, specimens with dimensions of 2 mm \times 2 mm \times 3.5 mm, prepared by electro-discharge machining, were taken both longitudinally and transversely to the growth direction and were tested in a flowing Ar/H $_2$ atmosphere using a Zwick/Roell Z100 electro-mechanical testing machine equipped with a Maytec furnace. The yield stresses were measured by the 0.2% offset method.

3. Results & Discussion

3.1. Microstructures

Specimens for microstructure analysis were cut by EDM from the directionally solidified rods and analyzed via SEM coupled with EDX as well as X-ray analysis. Representative micrographs of the DS Mo-34TiC and Mo-27ZrC alloy are shown in Figure 1. For the present alloys, X-ray diffraction measurements, shown in Figure 2, confirm the existence of the Mo solid solution phase (light grey phase) and ceramic phases TiC/ZrC (dark grey). Table 1 summarizes the corresponding fraction of the microstructural constituents for the alloys investigated, as obtained from Rietveld refinement.

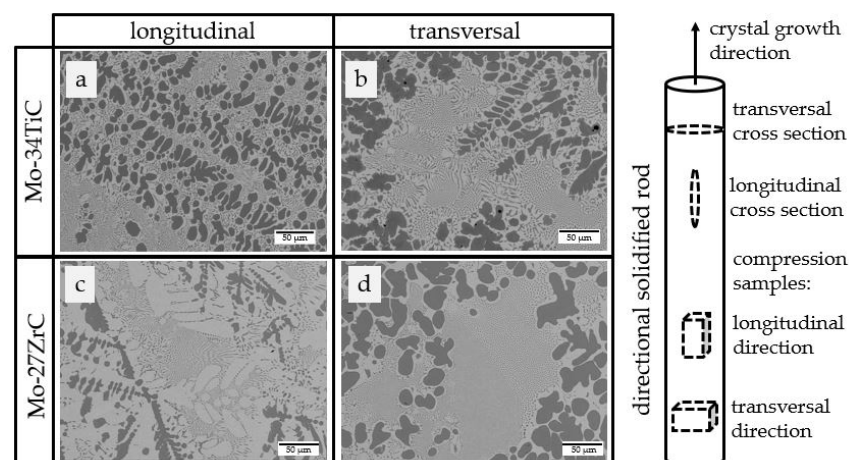


Figure 1. SEM-BSE images of Mo-34TiC and Mo-27ZrC in longitudinal and transversal section, representing eutectic colonies as well as dendritic regions. The Mo solid solution is the bright grey phase, whereas TiC and ZrC are depicted as the dark grey phases.

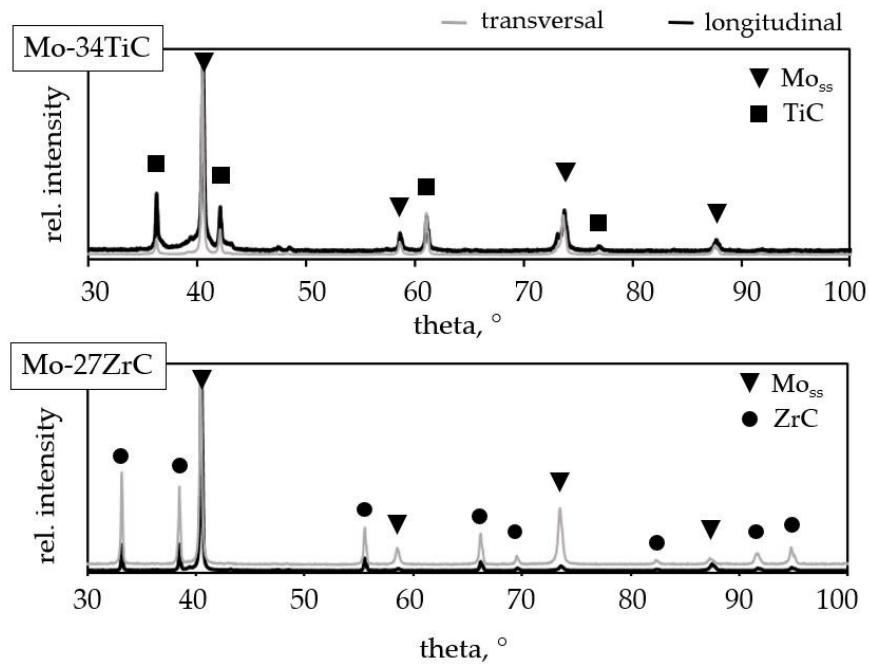


Figure 2. X-ray diffraction data for alloy Mo-34TiC and Mo-27ZrC, representing the existence of two phases in the composites: Mo_{ss}, TiC/ZrC.

Table 1. Microstructural features of the Mo-XC alloys compared with literature.

Alloy	Ceramic Phase Fraction Derived from Rietveld Refinement		Fracture Toughness MPa m ^{1/2}
	at.%	vol.%	
Mo-34TiC		41	~16
Mo-27ZrC		45	~26
Mo [22]		-	24
TiC [6,23]		-	2... 5
ZrC [10–12]		-	1... 4
Mo-50TiC [2]		-	9
Mo-13.9Zr-13.2C [9]		-	20

Figure 1a shows the microstructure for Mo-34TiC parallel to growth direction (longitudinal) consisting of near-eutectic Mo/TiC colonies elongated along the growth direction as well as larger dendritically grown TiC phases. Hence, near-eutectic alloy composition is achieved wherein areas of primarily solidified TiC phases are embedded in a Mo solid solution (Mo_{ss}) phase. Following the solidification sequence, eutectic cells form from the residual melt. Figure 1b represents a cross section of normal to growth direction (transversal), where equiaxed eutectic colonies and dendritic phase regions with different size and shape are observed. Figure 1c depicts the microstructure of the Mo-27ZrC alloy, where especially in the longitudinal section, larger Mo_{ss} regions appear in addition to larger ZrC phase regions as well as eutectic regions of Mo/ZrC. As can be seen in Figure 1d, the primarily solidified ZrC is surrounded by a fine eutectic structure.

Typically, powder metallurgically processed alloys suffer from a very high oxygen content in the range of 1500 ppm or even higher [24,25], which will cause embrittlement leading to higher BDTs. The zone melting process as used for this study typically results in a higher purity of alloys, especially in terms of interstitial elements such as oxygen. The protective He atmosphere during the directional solidification process could be one possible reason for the low impurity contents in ZM alloys, as explained by Hasemann et al. [19].

3.2. Mechanical Properties

3.2.1. Fracture Toughness

In order to evaluate the fracture toughness of each composite, three-point bending tests in the SEVNB method were carried out at room temperature. Specimens for bending tests were cut by EDM parallel to the growth direction and tested in a transversal section. The representative load-displacement curves in Figure 3 characterize the crack sensitivity, i.e., fracture toughness, of the Mo-XC composites.

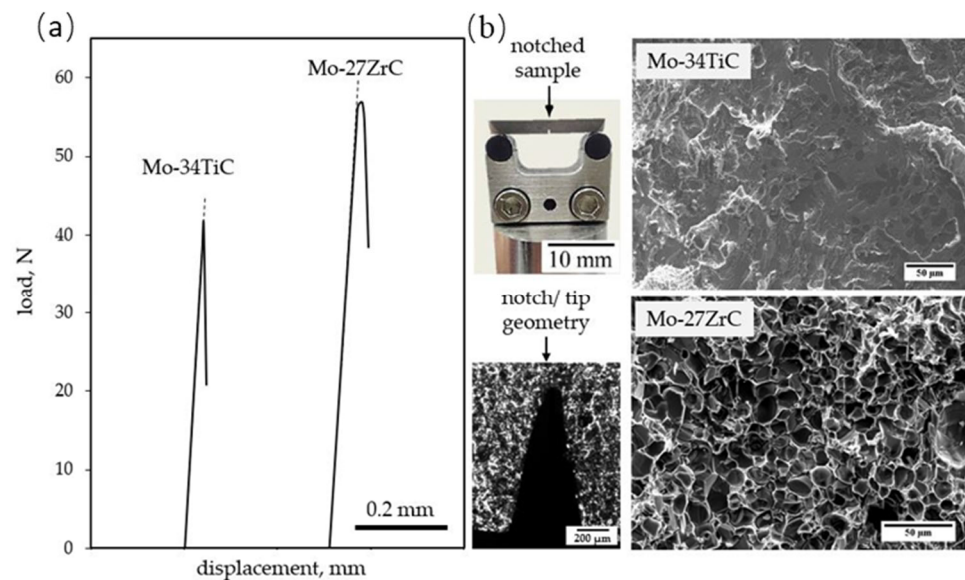


Figure 3. (a) Representative load-displacement curves of Mo-TiC/ZrC composites obtained by three-point bending test at room temperature perpendicular to growth direction; (b) fracture surfaces after cracking.

The curves demonstrate a higher bending strength of Mo-27ZrC compared with Mo-34TiC as well as the different crack modii. Similar to observations by Suzuki et al. [10], it can be determined that for Mo-27ZrC, the load-displacement curve displays non-linear behavior around the maximum load, indicating stable crack growth at an early stage of fracture. In contrast, the Mo-34TiC alloy only shows linear behavior, which is probably due to the absence of stable crack growth; i.e., catastrophic fracture. The different crack modii are illustrated by the SEM images of fracture surfaces shown in Figure 3. While the fracture surface for Mo-27ZrC shows ductile fracture behavior, brittle fracture by transgranular cleavage is clearly evident for Mo-34TiC. The values of fracture toughness K_{Ic} for the present alloys Mo-27ZrC and Mo-34TiC are mentioned in Table 1, with $26 \text{ MPa m}^{1/2}$ and $16 \text{ MPa m}^{1/2}$, respectively. It can be concluded that the superior fracture toughness of the Mo-27ZrC alloy is influenced by various parameters. Previous studies indicate that the amount of the Mo_{ss} phase, the chemical composition of this phase and its distribution has a significant impact on the cracking behavior. With a value of $24 \text{ MPa m}^{1/2}$ [22], this material shows a superior fracture toughness compared with monolithic TiC ($2 \dots 5 \text{ MPa m}^{1/2}$ [6,23]) and ZrC ($1 \dots 4 \text{ MPa m}^{1/2}$ [11–13]); therefore, it is the phase with the higher crack arrest capacity, as shown in previous studies [26]. As shown in Figure 1, the existence of large Mo_{ss} phases regions as well as eutectic Mo/ZrC regions with lamellar microstructure also plays an important role. In general, if compared with literature data for alloys with similar chemical compositions, the alloys presented in this work show superior fracture toughness. For Mo-27ZrC, the fracture toughness is even higher than the $20 \text{ MPa m}^{1/2}$ presented by Suzuki et al. [10] for eutectic Mo-13.9Zr-13.2C processed via directional solidification. It is assumed that this is caused by the significantly higher proportion of enlarged Mo_{ss} regions. Despite the linear load-displacement behavior according to non-stable crack growth as mentioned above, the alloy Mo-34TiC shows competitive fracture toughness compared

with values from the literature; e.g., around $9 \text{ MPa m}^{1/2}$ for powder metallurgically (PM) processed Mo-50TiC [2].

3.2.2. Compressive Strength

By using constant displacement tests at a nominal strain rate of $1 \cdot 10^{-4} \text{ s}^{-1}$ in uniaxial compression at temperatures up to $1000 \text{ }^\circ\text{C}$, the compressive strength and plastic deformability was analyzed for the present alloys. For the measurements, specimens were cut via EDM from the DS rods, both longitudinal and transversal to the growth direction (as sketched in Figure 1). The results are shown in Figure 4, representing the yield strength (by the 0.2 offset method) and plastic strain as a function of temperature. Regarding the yield strength for both the Mo-34TiC and Mo-27ZrC alloys, the compressive strengths in the transversal section are almost constant, whereas the compressive strengths in the longitudinal section decrease with increasing temperatures. These results clearly show the effect of the anisotropy in the DS microstructure, having globular phase regions in the traverse section and elongated structures in the direction of crystal growth on the mechanical properties. Accordingly, it is obvious that the deformation behavior perpendicular to the lamellar structure (transversal compression sample) can be limited, since the microstructural interruptions occur much more frequently transverse to the fiber direction than longitudinal to it. Even at higher temperatures, where increased diffusion occurs, the barrier effect perpendicular to the lamellar microstructure remains, whereas bypassing the phases in the longitudinal direction becomes easier with increasing temperatures.

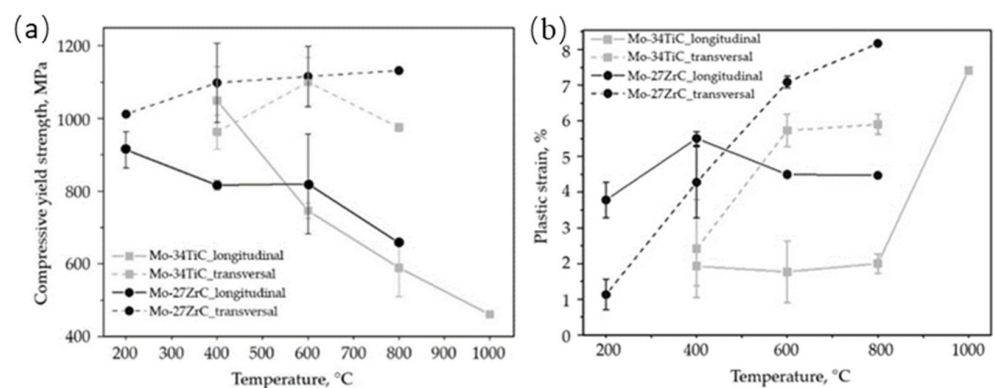


Figure 4. (a) Results of uniaxial compression tests on Mo-XC composites, representing the compressive yield strength vs. temperature; (b) the plastic strain vs. temperature.

A comparison of the yield strength of the Mo-34TiC alloy at $600 \text{ }^\circ\text{C}$, with test results for a PM Mo-23.5TiC alloy reported by Kurishita et al. [4] shows that the results obtained from the zone melting method are competitive. Thus, the Mo-23.5TiC alloy shows a yield strength around 1400 MPa , whereas the Mo-34TiC achieved a value of 1100 MPa . However, the Mo-23.5TiC alloy benefits from its homogeneous lamellar eutectic microstructure, while the large Mo_{ss} phase regions in Mo-34TiC weaken the alloy; however, they improve the ductility. The plastic deformation for the Mo-34TiC alloy, tested in the longitudinal section, significantly increases at $1000 \text{ }^\circ\text{C}$, which indicates that the BDTT is between $800 \text{ }^\circ\text{C}$ and $1000 \text{ }^\circ\text{C}$; this is typical for Mo alloys with high volume fractions of the Mo_{ss} phase.

In direct comparison, the Mo-27ZrC alloy shows a more promising performance in high temperature compression, since the temperature dependence of the yield strength of the transversal specimen is lower and it allows much more plastic deformation than Mo-34TiC. In this context, the somewhat higher proportion of the Mo_{ss} phase and the distribution of eutectic regions display a decisive impact.

4. Conclusions

The present investigations focused on the mechanical properties of directionally solidified Mo-XC alloys ($X = \text{Ti, Zr}$). Finally, the following conclusions can be drawn:

1. The cross sections of Mo-34TiC and Mo-27ZrC show microstructures with eutectic colonies with preferred orientation as well as coarse dendritic regions;
2. The fracture toughness of 26 MPa m^{1/2} for the Mo-27ZrC alloy is higher compared with Mo-34TiC (16 MPa m^{1/2}), affected by the homogeneity and fraction of the Mo_{ss} phase. The reasons for the comparatively high values are the high crack energy dissipation at the phase boundaries (testing the samples perpendicular to growth direction), the homogeneous distribution of the Mo_{ss} phase and acceptable values for the oxygen content being similar to those shown in studies by Bolbut et al. [20]. This indicates that stable crack growth at an early stage of fracture resulted in a superior fracture performance of Mo-27ZrC;
3. Uniaxial compression tests on longitudinal and transversal specimens displays anisotropic deformation behavior. A specimen in the transversal section shows higher yield stresses, whereas a specimen in the longitudinal section offers a decrease of strength with increasing temperatures; and
4. A specimen tested in the transversal section shows a higher ductility between 400 °C and 800 °C. Both longitudinal samples show a plateau-like plastic strain at temperatures lower than 800 °C, while the potential of plasticity is higher in Mo-27ZrC. The longitudinal sample of Mo-34TiC seems to have a BDTT between 800 °C and 1000 °C.

Author Contributions: Conceptualization, formal analysis, data curation, writing—original draft preparation, visualization, J.B.; investigation, D.B.; directional solidification of samples, I.B.; writing—review and editing, supervision, project administration, funding acquisition, M.K. All authors have read and agreed to the published version of the manuscript.

Funding: This research was funded by the DFG graduate school 1554 “Micro-macro interactions in structured media and particle systems” (funding number: 83477795).

Institutional Review Board Statement: Not applicable.

Informed Consent Statement: Not applicable.

Data Availability Statement: Not applicable.

Acknowledgments: Funding through the German Research Foundation (DFG), as part of the “Major Research Instrumentation Programme” (grant number: INST 272/281-1 FUGG) is gratefully acknowledged (Bruker D8 Discover XRD). The authors gratefully acknowledge Ulf Betke (OVGU Magdeburg) for conducting the Rietveld refinement.

Conflicts of Interest: The authors declare no conflict of interest.

References

1. Heumüller, H. Refraktärmetalle—Schlüsselwerkstoffe für die Hightech-Industrie. *World Metall.—ERZMETALL* **2008**, *61*, 352–389.
2. Cédât, D.; Rey, C.; Clavel, M.; Schmitt, J.H.; Le Flem, M.; Allemand, A. Microstructural characterization of a composite Mo reinforced by 25 at.% TiC. *J. Nucl. Mater.* **2009**, *385*, 533–537. [[CrossRef](#)]
3. Kohyama, A.; Igata, N. Surface radiation damage in Mo-TiC eutectic alloy and TiC bombarded by Ar⁺ and He⁺ Ions. *J. Nucl. Mater.* **1981**, *103*, 415–420. [[CrossRef](#)]
4. Kurishita, H.; Shiraishi, J.; Matsubara, R.; Yoshinaga, H. Measurement and Analysis of the Strength of Mo-TiC Composites in the Temperature Range 285 K–2270 K*. *Trans. Jpn. Inst. Met.* **1987**, *28*, 20–31. [[CrossRef](#)]
5. Hiraoka, Y. Strengths and ductility of Mo-TiC alloys after secondary recrystallization. *Int. J. Refract. Met. Hard Mater.* **2003**, *21*, 265–270. [[CrossRef](#)]
6. Le Flem, M.; Allemand, A.; Urvoy, S.; Cédât, D.; Rey, C. Microstructure and thermal conductivity of Mo-TiC cermets processed by hot isostatic pressing. *J. Nucl. Mater.* **2008**, *380*, 85–92. [[CrossRef](#)]
7. Cédât, D.; Libert, M.; Le Flem, M.; Fandeur, O.; Rey, C.; Clavel, M.; Schmitt, J.-H. Experimental characterization and mechanical behaviour modelling of molybdenum-titanium carbide composite for high temperature applications. *Int. J. Refract. Met. Hard Mater.* **2009**, *27*, 267–273. [[CrossRef](#)]
8. Suzuki, T.; Nomura, N.; Yoshimi, K.; Hanada, S. Microstructure and Creep of Mo-ZrC In-situ Composite. *Mater. Trans. JIM* **2000**, *41*, 1164–1167. [[CrossRef](#)]
9. Suzuki, T.; Matsumoto, H.; Nomura, N.; Hanada, S. Microstructures and fracture toughness of directionally solidified Mo-ZrC eutectic composites. *Sci. Technol. Adv. Mater.* **2002**, *3*, 137–143. Available online: <http://www.elsevier.com/locate/stam> (accessed on 30 September 2022). [[CrossRef](#)]

10. Landwehr, S.E.; Hilmas, G.E.; Fahrenholtz, W.G.; Talmy, I.G. Processing of ZrC-Mo cermets for high-temperature applications, part I: Chemical interactions in the ZrC-Mo system. *J. Am. Ceram. Soc.* **2007**, *90*, 1998–2002. [[CrossRef](#)]
11. Landwehr, S.E.; Hilmas, G.E.; Fahrenholtz, W.G.; Talmy, I.G.; Wang, H. Thermal properties and thermal shock resistance of liquid phase sintered ZrC-Mo cermets. *Mater. Chem. Phys.* **2009**, *115*, 690–695. [[CrossRef](#)]
12. Landwehr, S.E.; Hilmas, G.E.; Fahrenholtz, W.G.; Talmy, I.G.; DiPietro, S.G. Microstructure and mechanical characterization of ZrC-Mo cermets produced by hot isostatic pressing. *Mater. Sci. Eng. A* **2008**, *497*, 79–86. [[CrossRef](#)]
13. Ohser-Wiedemann, R.; Weck, C.; Martin, U.; Müller, A.; Seifert, H.J. Spark plasma sintering of TiC particle-reinforced molybdenum composites. *Int. J. Refract. Met. Hard Mater* **2012**, *32*, 1–6. [[CrossRef](#)]
14. Takida, T.; Mabuchi, M.; Nakamura, M.; Igarashi, T.; Doi, Y.; Nagae, T. The Role of Dispersed Particles in Strengthening and Fracture Mechanisms in a Mo-ZrC Alloy Processed by Mechanical Alloying. *Metall. Mater. Trans. A* **2000**, *A31*, 715–721. [[CrossRef](#)]
15. Takida, T.; Mabuchi, M.; Nakamura, M.; Igarashi, T.; Doi, Y.; Nagae, T. Mechanical properties of a ZrC-dispersed Mo alloy processed by mechanical alloying and spark plasma sintering. *Mater. Sci. Eng. A* **2000**, *276*, 269–272. [[CrossRef](#)]
16. Takida, T.; Kurishita, H.; Mabuchi, M.; Igarashi, T.; Doi, Y.; Nagae, T. Mechanical properties of fine-grained, sintered molybdenum alloys with dispersed particles developed by mechanical alloying. *Mater. Trans.* **2004**, *45*, 143–148. [[CrossRef](#)]
17. Yoshimi, K.; Nakamura, J.; Kanekon, D.; Yamamoto, S.; Maruyama, K.; Katsui, H.; Goto, T. High-Temperature Compressive Properties of TiC-Added Mo-Si-B Alloys. *JOM* **2014**, *66*, 1930–1938. [[CrossRef](#)]
18. Nakamura, J.; Kanekon, D.; Yoshimi, K. Characterization of Mo/Mo₂C interface in MoSiBTiC alloy. *Mater. Lett.* **2016**, *180*, 340–343. [[CrossRef](#)]
19. Hasemann, G.; Bogomol, I.; Schliephake, D.; Loboda, P.I.; Krüger, M. Microstructure and creep properties of a near-eutectic directionally solidified multiphase Mo-Si-B alloy. *Intermetallics* **2014**, *48*, 28–33. [[CrossRef](#)]
20. Bolbut, V.; Bogomol, I.; Bauer, C.; Krüger, M. Gerichtet erstarrte Mo-Zr-B-Legierungen: Directionally solidified Mo-Zr-B alloys. *Materwiss Werksttech* **2017**, *48*, 1113–1124. [[CrossRef](#)]
21. Becker, J.; Betke, U.; Hoffmeister, M.; Krüger, M. Density Reduction of Mo-Si-B Alloys by Vanadium Alloying. *JOM* **2018**, *70*, 2574–2581. [[CrossRef](#)]
22. Sturm, D.; Heilmaier, M.; Schneibel, J.H.; Jéhanno, P.; Skrotzki, B.; Saage, H. The influence of silicon on the strength and fracture toughness of molybdenum. *Mater. Sci. Eng. A* **2007**, *463*, 107–114. [[CrossRef](#)]
23. Hunger, H.-J. *Werkstoffanalytische Verfahren*; Deutscher Verlag für Grundstoffindustrie: Leipzig, Germany, 1995.
24. Krüger, M.; Franz, S.; Saage, H.; Heilmaier, M.; Schneibel, J.; Jéhanno, P.; Böning, M.; Kestler, H. Mechanically alloyed Mo-Si-B alloys with a continuous α -Mo matrix and improved mechanical properties. *Intermetallics* **2008**, *16*, 933–941. [[CrossRef](#)]
25. Krüger, M.; Schliephake, D.; Jain, P.; Kumar, K.S. Effects of Zr Additions on the Microstructure and the Mechanical Behavior of PM Mo-Si-B Alloys. *JOM* **2013**, *65*, 301–306. [[CrossRef](#)]
26. Becker, J.; Krüger, M. Impact of phase distribution on the fracture toughness of high temperature resistant Mo-Si-B alloys. *Pract. Metallogr.* **2015**, *52*, 295–313. [[CrossRef](#)]